Special Issue of the International Conference on Research and Applications of Plasmas (PLASMA-2019)

Laser-Target Experiments at PALS for Deuterium Plasma Beam Fusion

J. Krása[a,*], D. Klír[b], J. Cikhardt[b,c], M. Pfeifer[a,c], H. Hora[d,e], M. Krupka[a,c,f], K. Řezáč[b], R. Dudžák[a,c], J. Dostál[a,c], T. Burian[a,c], M. Krůs[c], J. Skála[a], K. Jungwirth[a], Z. Rusiniak[g], T. Pisarczyk[g] and T. Chodukowski[g]

[a] *Institute of Physics of the Czech Academy of Sciences, Prague, Czechia*
[b] *Faculty of Electrical Engineering, Czech Technical University in Prague, Prague, Czechia*
[c] *Institute of Plasma Physics of the Czech Academy of Sciences, Prague, Czechia*
[d] *HB11 Energy P/L, 11 Wyndora Ave., Freshwater, NSW 2096, Australia*
[e] *Department of Theoretical Physics, University of NSW, Sydney, Australia*
[f] *Faculty of Nuclear Sciences and Physical Engineering, Czech Technical University in Prague, Prague, Czechia*
[g] *Institute of Plasma Physics and Laser Microfusion, Warsaw, Poland*

Doi: 10.12693/APhysPolA.138.579 *e-mail: krasa@fzu.cz

The Prague Asterix Laser System (PALS) is a terawatt iodine laser (1.2 kJ, 350 ps, 1315 nm), designed to deliver irradiance on target of about 3×10^{16} W/cm^2. The PALS laser together with a Ti:sapphire laser (1 J, 50 fs, 800 nm) is used for experiments allowing femtosecond probing of laser-produced plasma. We present an experimental study of emission of hot electrons, fast ions and fusion neutrons generated through the ^{2}H(d;n)^{3}He fusion reaction of deuterons. During the laser–plasma interaction and plasma expansion, a multi-population of electrons appears. Non-isotropic emission of fast as well as thermal electrons is typical for the interaction of nanosecond laser radiation with plasma. The production of relativistic electrons makes it possible to accelerate protons to MeV energy and generate fusion neutrons via fusion reactions. The DD-neutron yield is compared to yields obtained from other experiments. Depending on the energy of the laser pulse, it is shown that the competition of laser contrast and laser pulse intensity sets a fundamental constraint on the ion emission and the resultant neutron yield performance of deuterated targets.

topics: laser–plasma acceleration of electrons and ions, self-focussing in plasmas, neutrons

1. Introduction

A number of laser facilities for laser fusion research have been built around the world [1]. Apart from the thermonuclear mechanism, DD or DT fusion neutrons can be produced by beam–target mechanism. In this case, the interaction of laser pulses with deuterated targets at relativistic intensities and below the relativistic threshold accelerates ions to MeV energies [2–6]. Then, accelerated ion beams may fuse with target ions.

In 1998, a significant number of non-thermal neutrons up to 7×10^7 n/sr were produced with energy of 20 J and intensity of 8×10^{18} W/cm^2 [7]. In 1999, a deuterated polyethylene target exposed to intensity of a few 10^{19} W/cm^2 emitted 10^7 neutrons for laser energy of 7 J at 529 nm [3].

A comparison of the number of fusion neutrons generated in many laser-driven experiments showed that the neutron yield under specific experimental conditions was nearly three to four orders of magnitude higher than under standard conditions associated with nanosecond laser–plasma interaction, as Fig. 3 in [5] shows. It was shown [8] that the interaction area had a low temperature, which indicated the non-local thermodynamic equilibrium (non-LTE) conditions under which the nuclear fusion is driven by laser-accelerated ion beams in the laser-produced plasma.

In this paper, we present the summary about the approach that realizes a substantial increase in the neutron yield of a laser-driven DD reaction. It is based on the measured high acceleration of plasma using not only the PALS iodine laser but also other femto-, pico- and nanosecond lasers. In this work, which is a review of important experimental results obtained at the PALS facility, the partial results will be presented regardless of the target material but to highlight the observed phenomena. We note that a review of other experiments performed at the PALS facility is given in [9].

2. Experimental arrangement

Experimental studies of intense laser interactions with targets of different materials were carried out at the PALS facility. The iodine high-power laser system operated at fundamental wavelength $\lambda = 1.315$ μm can deliver energy up to ≈ 800 J on targets in a pulse duration of ≈ 350 ps. The targets were the deuterated polyethylene CD_2 (PED) flat slabs of 0.2–0.5 mm in thickness and Mo foils of 6 μm in thickness. Perpendicular or oblique (at 30°) target irradiation was used in these experiments. The minimum diameter of the focal spot of ≈ 70 μm provides a maximum value $I\lambda^2 \approx 5 \times 10^{16}$ W cm^{-2} μm^2.

Characteristics of emitted ions were measured with the use of ion collectors, CR-39 solid-state nuclear track detectors and gafchromic films (RCF), types HD-V2 and EBT3. Ion detectors were wrapped with a 7 to 14 μm Al foil to prevent low-energy X-ray radiation, scattered laser light and to slow down ions in striking the foil detectors. The yield of neutrons produced through the fusion reaction ^{2}H(d,n)^{3}He was detected with the use of an Ag activation counter and bubble detectors.

The electron energy distribution function (EEDF) was measured with the use of magnetic dipole spectrometers equipped with a pair of magnets producing a uniform magnetic field equal to 160 mT and electron sensitive image plate, type Fuji BAS SR2040, calibrated for electrons in [10]. The spectrometers were designed to cover electron energy in the range from 100 keV to 5 MeV. Interferometric studies of plasma dynamic during interaction and post-interaction phases are based on the recently developed system of precise pulse synchronization between the PALS single-shot large-scale laser exploiting an acoustic-optical modulator and a 45 fs, 25 TW Ti:sapphire (Ti:Sa) [11]. The Ti:Sa beam was employed as a probing beam of the plasma produced with the PALS laser. Sequences of three-frame interferograms timed with respect to the intensity maximum of the PALS laser enable us to observe the evolution of subcritical corona and to determine the space electron density distribution [12]. Refraction of the probing beam in the strong density gradients limited the observation to regions with electron density less than 10^{20} cm^{-3}.

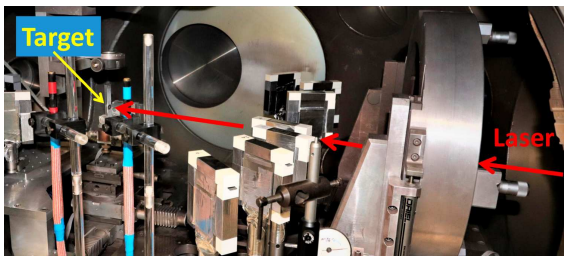

Fig. 1. View into the PALS interaction chamber. The laser pulse coming from the right side is focused by an aspheric lens on the target surface (red line). The minimum diameter of the focus spot is 70 μ m. There are 9 electron energy spectrometers (white horns boxes) in the chamber for measuring the angular distribution of the energy spectrum of electrons. On the left are the holders with EMP antennas.

The target current, which substitutes hot electrons which escaped the plasma and, thus, neutralizes the positive charge created in the plasma and target, was measured using an inductive target probe [13].

Figure 1 shows a view into the PALS interaction chamber equipped with electron spectrometers and antennas detecting high frequency electromagnetic pulses (EMP) emitted during the neutralization of the target positive charge.

3. Experimental results

3.1. Emission of hot electrons

The expansion of the laser-generated plasma into the interaction chamber is associated with the separation of charges. This space-charge effect self-consistently produces an ambipolar electric field whose amplitude is controlled by the energy and number of electrons constituting the tail of EEDF. These regions of positive and negative charges form a double layer which continues to develop during their expansion into the vacuum. Simultaneously with the expanding plasma, formations of potential on the target and of the current flowing from the ground to the target have been observed. It is caused by electrons from the tail of EEDF that overcome the plasma potential barrier and escape the plasma [14]. Using a number of magnetic dipole spectrometers surrounding the target in a distance of about 30–40 cm we obtained an angular dependence of EEDF of hot electrons. Figure 2 shows an example of three EEDFs of hot electrons emitted from the front surface of a Mo target in the direction of −39°, −27° and 17° with respect to the laser beam vector. The Mo foil of 6 μm in thickness was exposed to 3×10^{16} W/cm^2 intensity. Although the laser-produced plasma with two electron populations is commonly presented in many papers as a typical phenomenon [15], Fig. 2 shows experimentally observed multi-peaked energy distribution functions of electrons emitted anisotropically into the vacuum.

Our experiments have also shown that the EEDFs did not exhibit a shape which would have met a one-temperature Maxwell–Jüttner distribution [16]:

$$f(\gamma) = \frac{\gamma\sqrt{\gamma^2-1}}{\theta K_2\left(\frac{1}{\theta}\right)} \exp\left(-\frac{\gamma}{\theta}\right), \qquad (1)$$

where $\theta = k_B T_h / mc^2$ and K_2 is the modified Bessel function of the second kind. One of the reasons of this discrepancy is the occurrence of multiple-electron populations, as Fig. 3 shows.

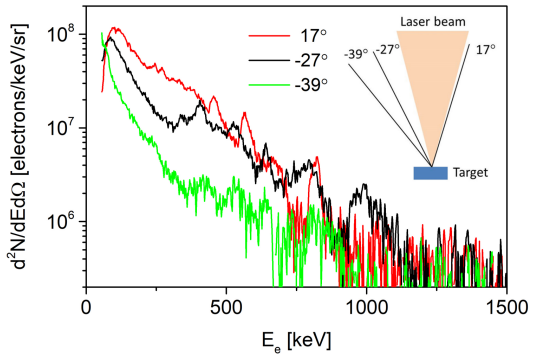

Fig. 2. Energy distribution of hot electrons emitted from the front target surface in the direction of $-39°$, $-27°$, and $-17°$ with respect to the laser beam vector. Mo foil of 6 μ m in thickness was irradiated to 3×10^{16} W/cm^2 laser intensity.

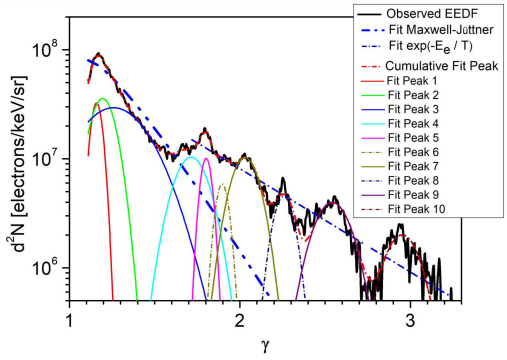

Fig. 3. Analysis of EEDF with the use of fitting of the observed EEDF to the Maxwell–Jüttner function (7), $\exp(-E_e/T)$, and to a set of 10 normal distributions (8).

The fit of the experimentally obtained EEDF to the single Maxwell–Jüttner distribution function gives the electron temperature of 77 keV, but gives no information about hot electrons for the Lorenz factor $\gamma \geq 1.6$. Hence, the EEDF was fitted to the second distribution that gave the temperature value of 201 keV. It is obvious that even the two-temperature model does not give a satisfactory fit. For this reason, the experimentally obtained EEDF with a number of visible peaks should be analysed in a different way.

In view of a balance between simplicity and accuracy of the analysis and in accordance with results presented by Sherlock in [17], a few peaks in the EEDF can be revealed by fitting a sum of shifted-Gaussian functions $\sum f_i(\gamma)$ to the observed data, where

$$f_i(\gamma) = C_i \exp\left(-0.5\left(\frac{\gamma - \gamma_{i-\mathrm{peak}}}{\Delta\gamma_i}\right)^2\right) g_i(\vartheta), \tag{2}$$

C_i is the normalisation constant, $\gamma_{i-\mathrm{peak}}$ is the i-th peak centre, $\Delta\gamma_i$ is the standard deviation (energy spread) and $g_i(\vartheta)$ is the angular component of the EEDF.

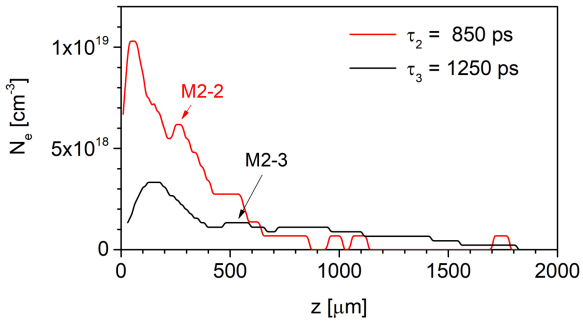

Fig. 4. Axial dependence of electron density for two times of 850 ps and 1250 ps related to the z-axis of Fig. 5.

The interpolation of the observed EEDF as a sum of ten normal distributions suggests that the multi-peaked structure of the EEDF should encapsulate a number of processes which occurred during the laser–plasma interaction. The sum of several independent processes controlling the production of hot electrons might lead to such a result that the observed EEDF tends to be a normal (Gaussian) distribution [18], which is generally stated when one is justified in expecting a Gaussian distribution. Although the individual peaks constituting the experimentally obtained EEDF do not need to be visibly separated, the multi-peaked structure of the EEDF is the reason why the observed electron spectra do not only show a clear shape of the Maxwell–Jüttner distribution but also indicate a complex process of plasma formation.

It has been recognized that the laser–plasma interaction is ruled by various self-focusing processes and by other collective phenomena affecting the absorption of laser radiation using laser pulses of high intensity [19, 20]. In this case, the energy distribution function might not take the form of a simple shape of the Maxwell or Maxwell–Jüttner distribution. The multi-peak structure of the EEDF should affect the characteristics of fast ions which can be accelerated by different electric fields and emitted in bursts, as reported in [21]. These bursts can be caused by the presence of kinetic mechanisms saturating the SRS growth in laser beam speckles with high local intensity, particularly at higher laser intensities [22]. The temporal evolution of SRS reflectivity exhibits a burst-like behaviour as the ion emission does.

The hot electrons can be produced due to the filamentation because the threshold intensity for them is reachable during the laser–plasma interaction, as shown in [16]. The time evolution of $n_e(r, z, \Delta t)$, which is computed from the femtosecond interferograms obtained at different times related to the laser intensity maximum, exhibits a local peak in $n_e(0, z)$, i.e., a local plasma bunch [12, 16]. Figure 4 shows visible peaks labelled as M2-2 and M2-3 in $n_e(0, z)$ at a distance of ≈ 250–550 μm from the front surface of

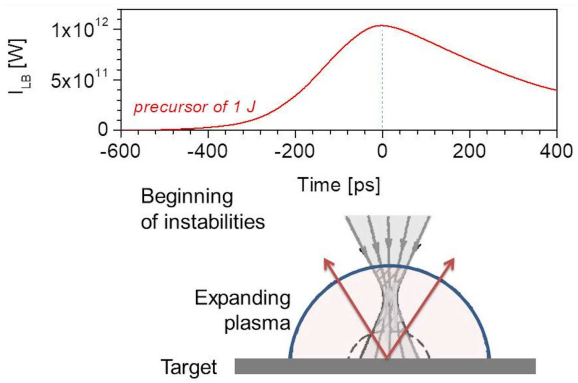

Fig. 5. The upper diagram shows a time profile of laser power reaching a maximum value of 1 TW at time 0, obtained using a streak camera. The plasma formation threshold in this experiment is about 10^4 W. The bottom sketch shows the process of self-focusing and defocusing of the laser beam in the produced plasma.

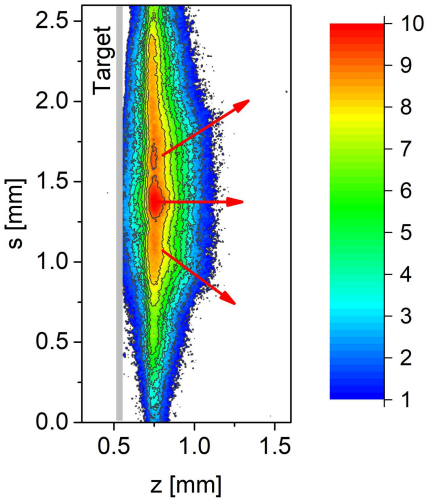

Fig. 6. X-ray visualization of Mo plasma at 1 ns after the impact of a 350 ps laser pulse. The 512-J laser pulse is normally incident from the right on the target foil of 6 μ m in thickness. The red arrows indicate the main directions of plasma expansion in the vacuum.

the Mo foil at times of 850 and 1250 ps, respectively. The local bunches of electrons gradually disappearing after the laser–plasma interaction can be produced during the laser–plasma interaction when the process of self-focusing–defocusing–self-focusing of the laser beam in the expanding plasma occurs. The process of self-focusing followed by defocusing is sketched in Fig. 5.

A similar space distribution showing local maxima in soft X-ray radiation emitted by the plasma expanding from the irradiated target surface into the vacuum can be obtained using a gated pinhole X-ray camera. Due to the fact that the X-ray pinhole camera used has a gate time of 3 ns, it is not possible to identify local plasma bunches as observed in the previous case, where the interferometry with the equivalent gate time of $\approx$ 50 fs was used. Nevertheless, Fig. 6 shows an example of X-ray image of the Mo plasma obtained at 1 ns after the laser-target interaction. This X-ray image clearly shows the complex radial emission profile, which is fundamentally different from the point-like source of radiation.

As Figs. 4 and 6 indicate, the different populations and different origins of the same species should be taken into account. These different populations can be identified by partial peaks resolved in the experimentally observed EEDF, as Fig. 3 shows, or can be achieved by measuring the ionic emission temporal profiles, i.e., time of flight (TOF) spectra indicating the bursts of ions, as has been presented in [5]. These experimental results indicate the formation of multi-electron temperature plasma. The observed anisotropic peaked EEDFs indicate possible occurrence of bunches of hot electrons which passed through the plasma potential barrier.

3.2. Emission of fusion neutrons

The experimental observation of ion, as well as deuteron bursts have shown that the centre-of-mass energies decrease gradually with the increasing sequence number of the burst which is expressed in terms of the n-th burst starting at the shortest flight time (i.e., the highest centre-of-mass energy) of a burst, as it was described in [21]. Since the average N-TOF signal of fusion neutrons observed on-axis (i.e., in the laser vector direction) have FWHM ranging from about 1.3 to about 2.7 MeV and maxima at a time corresponding to the neutron energy of $\approx$ 2.45 MeV, then the anticipated shift of the n-th peak of N-TOF due to the Doppler effect reflecting the velocities of the reactants is insignificant [5]. The observed N-TOF spectra allow to determine the equivalent temperature of fusing deuterons by using the formula $\Delta E_{\mathrm{N-DD}} = 82.5\sqrt{T}$ [23, 24], where $\Delta E_{\mathrm{N-DD}}$ is the energy spread of DD-neutrons determined from $\Delta\tau_{\mathrm{FWHM}}$ of the N-TOF spectrum and T is the temperature of fusing ions. The value of T estimated from the average broad N-TOF spectra was $\approx$ 100 keV. This value can be overestimated because the neutrons can also be generated by a burst emission mechanism which was observed in the ion emission [5]. In this case, the temperature should decrease to a few tens of keV because that the corresponding values $\Delta E_{\mathrm{N-j-burst}}$ of partial bursts are lower than the "total" $\Delta E_{\mathrm{N-DD}}$. As the emission of partial bursts of ions has a cascading form with a delay between the bursts of $\approx$ 4 ps to $\approx$ 14 ps, a similar form of the accompanying emission of fused neutrons can be expected. Nevertheless, the full-time evolution of the neutron bursts cascade including the partial fusion burn times can be hardly uncovered from the mean N-TOF signal due to the averaging of shot-to-shot fluctuations, which are inherent

to the burst emission mechanisms. Similar average N-TOF signal and, thus, energy spectra of neutrons were reported by Norreys et al. [25], namely for the average intensity on target of 8×10^{18} W/cm^2. This intensity allows generating neutrons having energy distribution with FWHM of 680 keV.

The average N-TOF signal observed in the on-axis direction has FWHM ranging from ≈ 1.3 MeV to ≈ 2.7 MeV. If the beam of deuterons hits nucleons in the stationary target along the target surface normal, then the energy of neutrons outgoing from the ^{2}H(d,n)^{3}He reaction depends on the energy of the collided deuterons. The neutrons emitted in the forward direction with energy of 3.1 MeV were generated by deuterons collided with ≈ 250 keV energy, as can be estimated from the numerical modelling presented in [26]. These 250 keV deuterons also cause the emission of neutrons in the backward and radial directions with energies of ≈ 2 MeV and ≈ 2.5 MeV, respectively. Regarding the radial spectrum, if the fusion neutrons are generated only by deuterons hitting the target along its surface normal (forward direction) with the 250 keV energy, then the neutrons emitted in the radial direction should have a very narrow spectrum of about 2.51 ± 0.01 MeV, as estimated from [26]. However, the neutrons we observed in the radial direction have very broad spectrum, which is centred on the fusion energy fraction of 2.45 MeV carried by DD-neutrons, as similar spectra obtained on various other laser and plasma-focus devices show. Such broad spectra can be explained only by considering the deuterons impacting at various angles with respect to the laser-beam or plasma-focus axis, because they should interact with each other via "transverse" collisions of reacting nuclei that have radial velocity components.

It is also evident from the observed slow decrease in the on-axis N-TOF spectrum towards longer flight times that a significant number of forward neutrons arriving at 140 ns (i.e., at a FWHM level) and having the energy only of 1.3 MeV originated from another nuclear reaction, as D-^{12}C and ^{12}C-D producing neutrons with lower energies up to 2.4 MeV [5]. A smaller portion of these slower neutrons was slowed down by collisions with a "moderating' medium". However, the single-shot N-TOF signals [4, 5] converted into the energy spectra are very similar to the energy spectra produced from a CD_2 target exposed to the intensity of 3×10^{18} W/cm^2 as shown in [27].

It is remarkable that in these experiments we observed neutrons that were generated by the impact of deuterons on a borosilicate blast plate shielding the focusing optics. The observed fastest neutrons produced through the ^{11}B(d,n)^{12}C reaction with the Q-value of 13.73 MeV had energy > 13 MeV [4].

Apart from the instabilities influencing the energy transfer from the laser beam to fusing ions via generated hot electrons, the sharp focusing of the laser radiation on the target is one of

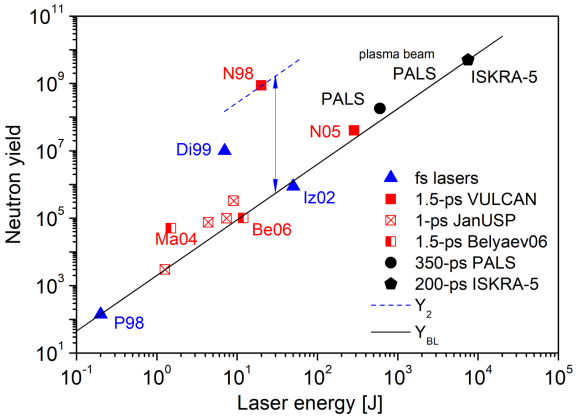

Fig. 7. Laser energy dependence of yield of fusion neutrons emitted from targets containing deuterium irradiated by femto- to 350 ns laser pulses. Data from: P98 [28], Ma04 [29], Iz02 [30], Di99 [3], Be06 [31], N05 [25], N98 [7], PALS [4, 5], ISKRA-5 [32].

the decisive factors affecting the neutron yield [5]. The maximum value of the neutron yield per laser energy, Y/E_L, was observed in the PALS facility to be $Y/E_L = 3.5 \times 10^5$ n/J, i.e., 2×10^8 neutrons for the average $E_L = 550$ J. This value falls between the higher efficiency values observed at the laser solid interactions driven by high laser intensities [4, 5].

Regardless of the number of nonlinear processes occurring during laser plasma interaction, such as self-focusing which can grow in plasma through thermal, relativistic and ponderomotive effects [16, 19], as well as parametric instabilities [22, 33, 34], the main parameter quantifying the laser system quality remains the neutron production efficiency Y/E_L. Figure 7 shows the laser energy dependence of the neutron yield, where only selected experiments giving the lowest and highest neutron yield are presented. The lowest laser energy efficiencies into neutron production are found to scale as $Y_{\mathrm{BL}} = 2000E^{1.65}$ [5]. The line representing the highest yield per laser energy (N98) is $Y_2 \cong 6 \times 10^6 E^{1.65}$. This diagram does not show other already published neutron gains, as other diagrams presented in [4, 5]. Here, we would like to draw attention to the influence of the laser beam contrast on the yield of fusion neutrons, namely the experiments carried out in the Vulcan laser facility [7, 25].

The most exceptional number of neutrons per steradian of 7×10^7 n/sr was reached at an intensity on target of 8×10^{18} W/cm^2 [7], see label N98 in Fig. 7. When the target was exposed to 400 J instead of 20 J, as in the Vulcan experiment N98 [7], and the focused intensity increased to 4×10^{20} W/cm^2, the neutron yields were going down to the values of around 2–40×10^6 neutrons per laser shot [25], see label N05. In this experiment, the laser pulse intensity

contrast ratio was $\approx 5 \times 10^{-8}$. It is therefore evident that a pre-pulse irradiating the target with the intensity of 10^{13} W/cm^2, which was higher than the plasma formation threshold, produced a pre-plasma with which the main 1 ps laser pulse interacted. Although it is difficult to estimate the influence of an uncontrollable pre-plasma on the ion acceleration and, thus, neutron yield, it can be assumed that both temperature and number of hot electrons are decreasing with the increasing level of pre-plasma [35]. The comparison of the N05 and PALS values of Y/E_L, which are $\approx 1 \times 10^5$ and $\approx 4 \times 10^5$, respectively, does not indicate any significant difference, although the Vulcan laser intensity was by a factor of ten thousand higher than the PALS intensity. Regardless of the differences in the interaction of ps- and ns-lasers with matter [25], one can deduce that it is just the interaction of the main laser pulse with the uncontrollable pre-plasma which can decrease the efficiency of ps- and sub-ps laser systems in generation of fusion neutrons. The lines Y_2 and Y_{BL} shown in Fig. 7 also indicate that the non-thermal properties of the ultra-high picosecond acceleration of plasma blocks by nonlinear-force acceleration could result in ten-thousand times higher fusion neutron production than when the laser volume interacts with the plasma produced [8]. Of course, there are other laser parameters and a number of processes forming the plasma that affect the neutron production efficiency Y/E_L.

The value of Y/E_L was increased by a factor of about 7.5 on the PALS experiment when a pitcher-catcher target configuration was applied [4]. In this experiment, the laser beam struck the $(\mathrm{CD_2})_n$ target at the angle of 30° and the plasma beam expanded from the front side of the target along the target surface normal into the vacuum to bombard catcher targets of 50–60 cm^2 area.

The implemented beam-target fusion configuration increased the resulted neutron yield to the value of 2×10^9, as marked in Fig. 7 with the label "PALS plasma beam". This result reveals that most of the deuterons, i.e., about 80%, having enough kinetic energy to enter the ^{2}H(d,n)^{3}He fusion reaction, are emitted from the primary target into the vacuum. This value of neutron yield allows us to calculate that the secondary target was bombarded by 2×10^{14} deuterons in the 0.5–2.0 MeV energy range. Assuming the mean energy of fusing deuterons of ≈ 1 MeV, the energy carried by these deuterons implies 5% conversion efficiency of the laser energy to fusing deuterons [4].

Although the beam-target fusion scheme on the PALS experiment reached $Y/E_L = 3 \times 10^6$ n/J, this value is still less than the Vulcan yield $Y/E_L = 4 \times 10^7$ n/J [7], that was achieved under conditions of sufficiently high contrast avoiding nearly the interaction of the pulse with the pre-plasma. We have to note that the value of the laser pulse intensity contrast ratio in not given in this work [7]. However, we can assume that the contrast of this 20-J Vulcan laser system [7] was better than the above mentioned 5×10^{-8} contrast of the 400-J Vulcan laser [26].

4. Conclusions

The use of various experimental techniques allowed us to observe and characterize the emission of relativistic electrons, MeV protons and deuterons from various targets exposed to intensity of $\approx 3 \times 10^{16}$ W/cm^2 delivered by the iodine laser PALS in pulses with the duration of 350 ps. The observed values of ion energy and temperature of hot electrons do not correlate with any of the temporally known corresponding models of plasma produced at this intensity, which do not account for possible nonlinear effects as the self-focusing of the laser beam causing the increase in the laser intensity. Nonlinear interaction of the laser beam with the plasma can lead to the appearance of plasma bunches that have been identified in the thermal plasma generated on the target surface by time-resolved femtosecond interferometry. In addition to these bunches of thermal plasma, a number of populations of hot electrons which passed through the plasma barrier were observed using electron spectrometers. The analysis of interferograms has also shown that the threshold intensity for both the thermal and relativistic filamentation is reachable during the laser–plasma interaction [16].

The PALS laser makes it possible to accelerate a large number of fast deuterons which can generate neutrons through the ^{2}H(d,n)^{3}He fusion reaction. The beam-target fusion experiment revealed that a number of 10^{14} of $>$ 500 keV deuterons escaped from the laser-produced plasma and carried out about 5% of laser energy deposited on the target.

The comparison of neutron yields obtained in PALS experiments with those achieved in other laser facilities shows that the greatest possible reduction in neutron yield is due to the very insufficient contrast ratio, so that the relativistic self-focusing cannot be prevented when ps and sub-ps laser pulses interact with the target [8].

Acknowledgments

The research leading to these results has received funding from the Czech Science Foundation (Grant No. 19-02545S), the Czech Republic's Ministry of Education, Youth and Sports — the projects: Prague Asterix Laser System (LM2015083) and Creating and Probing Dense Plasmas at the PALS Facility (CZ.02.1.01/0.0/0.0/16_013/0001552), the European Union's Horizon 2020 Research and Innovation Programme under Grant Agreement No. 654148 Laserlab-Europe.

References

[1] K. Mima, in: *Fusion Physics*, Eds. M. Kikuchi, K. Lackner, M. Q. Tran, International Atomic Energy Agency Vienna, Vienna 2012, p. 1043.

[2] T. Ditmire, J. Zweiback, V.P. Yanovsky, T.E. Cowan, G. Hays, K.B. Wharton, *Phys. Plasma* **7**, 1993 (2000).

[3] L. Disdier, J.-P. Garçonnet, G. Malka, J.-L. Miquel, *Phys. Rev. Lett.* **82**, 1454 (1999).

[4] D. Klir, J. Krasa, J. Cikhardt et al., *Phys. Plasma* **22**, 093117 (2015).

[5] J. Krasa, D. Klir, A. Velyhan et al., *Laser Part. Beams* **31**, 395 (2013).

[6] H. Daido, M. Yamanaka, K. Mima, K. Nishihara, S. Nakai, Y. Kitagawa, E. Miura, C. Yamanaka, A. Hasegawa, *Appl. Phys. Lett.* **51**, 2195 (1987).

[7] P.A. Norreys, A.P. Fews, F.N. Begx, A.R. Bell, A.E. Dangor, P. Lee, M.B. Nelson, H. Schmidt, M. Tatarakis, M.D. Cable, *Plasma Phys. Control. Fusion* **40**, 175 (1998).

[8] H. Hora, S. Eliezer, G.H. Miley, J.X. Wang, Y.X. Xu, N. Nissim, *Laser Part. Beams* **36**, 335 (2018).

[9] J. Ullschmied, *Rad. Eff. Def. Solids* **170**, 278 (2015).

[10] H. Chen, N.L. Back, T. Bartal et al., *Rev. Sci. Instrum.* **79**, 033301 (2008).

[11] J. Dostal, R. Dudzak, T. Pisarczyk et al., *Rev. Sci. Instrum.* **88**, 045109 (2017).

[12] T. Pisarczyk, S.Yu. Gus'kov, Z. Kalinowska et al., *Phys. Plasmas* **21**, 012708 (2014).

[13] J. Cikhardt, J. Krása, M. De Marco et al., *Rev. Sci. Instrum.* **85**, 103507 (2014).

[14] A. Poyé, J.-L. Dubois, F. Lubrano-Lavaderci et al., *Phys. Rev. E* **92**, 043107 (2015).

[15] G. Hairapetian, R.L. Stenzel, *Phys. Fluids B Plasma Phys.* **3**, 899 (1991).

[16] J. Krása, D. Klír, K. Řezáč et al., *Phys. Plasma* **25**, 113112 (2018).

[17] M. Sherlock, *Phys. Plasmas* **16**, 103101 (2009).

[18] A. Lyon, *Brit. J. Philos. Sci.* **65**, 621 (2014).

[19] W.L. Kruer, in: *Laser Program Annual Report*, 1984, Eds. M.L. Rufer, P.W. Murphy, Lawrence Livermore National Lab., CA (USA) 1985, p. 3.32.

[20] D. Batani, S. Baton, A. Casner et al., *Nucl. Fusion* **54**, 054009 (2014).

[21] J. Krása, A. Velyhan, K. Jungwirth, E. Krouský, L. Láska, K. Rohlena, M. Pfeifer, J. Ullschmied, *Laser Part. Beams* **27**, 171 (2009).

[22] G. Cristoforetti, L. Antonelli, S. Atzeni et al., *Phys. Plasmas* **25**, 012702 (2018).

[23] H. Brysk, *Plasma Phys. Control. Fusion* **15**, 611 (1973).

[24] B. Wolle, *Phys. Rep.* **312**, 1 (1999).

[25] P.A. Norreys, K.L. Lancaster, H. Habara et al., *Plasma Phys. Control. Fusion* **47**, L49 (2005).

[26] K. Rezac, D. Klir, P. Kubes, J. Kravarik, *Plasma Phys. Control. Fusion* **54**, 105011 (2012).

[27] A. Youssef, R. Kodama, H. Habara, K.A. Tanaka, Y. Sentoku, M. Tampo, Y. Toyama, *Phys. Plasmas* **12**, 110703 (2005).

[28] G. Pretzler, A. Saemann, A. Pukhov et al., *Phys. Rev. E* **58**, 1165 (1998).

[29] K.W. Madison, P.K. Patel, M. Allen, D. Price, R. Fitzpatrick, T. Ditmire, *Phys. Rev. A* **70**, 053201 (2004).

[30] N. Izumi, Y. Sentoku, H. Habara et al., *Phys. Rev. E* **65**, 036413 (2002).

[31] V.S. Belyaev, V.I. Vinogradov, A.P. Matafonov, V.P. Krainov, V.S. Lisitsa, V.P. Andrianov, G.N. Ignatyev, *Laser Phys.* **16**, 1647 (2006).

[32] A.V. Bessarab, V.A. Gaidash, G.V. Dolgoleva et al., *Sov. Phys. JETP* **75**, 970 (1992).

[33] O. Klimo, V.T. Tikhonchuk, *Plasma Phys. Control. Fusion* **55**, 095002 (2013).

[34] S. Weber, C. Riconda, *High Power Laser Sci. Eng.* **3**, e6 (2015).

[35] J. Peebles, M.S. Wei, A.V. Arefiev et al., *New J. Phys.* **19**, 023008 (2017).